Sains Malaysiana 55(2)(2026): 339-350
http://doi.org/10.17576/jsm-2026-5502-13

Effect of Sintering Temperature on $YBa_2Cu_3O_{7-\delta}$ Prepared via Modified Decomposition Method

(Kesan Suhu Pensinteran terhadap $YBa_2Cu_3O_{7-\delta}$ yang Disediakan melalui Kaedah Penguraian Terubah Suai)

NURHIDAYAH MOHD HAPIPI[1], SOO KIEN CHEN[1,2,*], ABDUL HALIM SHAARI[1], MOHD MUSTAFA AWANG KECHIK[1], KEAN PAH LIM[1], MUHAMMAD KASHFI SHABDIN[1], KAR BAN TAN[3], OON JEW LEE[4], SIEW HONG YAP[1], NUR HUMAIRA YASMIN MOHD ALIMI[1] & XIAO TONG HON[1]

[1]*Department of Physics, Faculty of Science, Universiti Putra Malaysia, 43400 UPM Serdang, Selangor, Malaysia*
[2]*Institute of Nanoscience and Nanotechnology (ION2), Universiti Putra Malaysia, 43400 UPM Serdang, Selangor, Malaysia*
[3]*Department of Chemistry, Faculty of Science, Universiti Putra Malaysia, 43400 UPM Serdang, Selangor, Malaysia*
[4]*Faculty of Science and Marine Environment, Universiti Malaysia Terengganu, 21030 Kuala Nerus, Terengganu, Malaysia*

Received: 14 October 2025/Accepted: 9 February 2026

ABSTRACT

In this study, $YBa_2Cu_3O_{7-\delta}$ (Y-123) high-temperature superconductors were synthesised via a modified thermal decomposition method using metal acetate precursors, with the sintering temperature varied between 920 °C and 980 °C. Phase formation, microstructure, and superconducting properties were systematically studied. Thermogravimetric analysis (TGA/DTG) showed a multi-step decomposition process, with final oxide formation occurring at temperatures above 500 °C. X-ray diffraction (XRD) confirmed Y-123 as the dominant phase, accompanied by impurity phases such as Y_2BaCuO_5 (Y-211) and $BaCuO_2$. Scanning electron microscopy (SEM) showed significant grain growth from 0.85 μm to 1.36 μm as the sintering temperature increased from 920 °C to 980 °C, which enhanced the grain connectivity in the sample. Electrical resistivity measurements showed that all samples exhibited a consistent onset critical temperature ($T_{c\text{-}onset}$) of 93.1 K, while the zero-resistance temperature ($T_{c\text{-}zero}$) increased from 75.1 K to 88.1 K as the sintering temperature increased from 920 °C to 960 °C. The improvement in superconducting performance is due to enhanced phase formation and increased grain connectivity. These findings indicate that optimisation of sintering temperatures is a key factor in improving the microstructure and superconducting properties of Y-123 samples.

Keywords: Sintering; superconductor; thermal decomposition; $YBa_2Cu_3O_{7-\delta}$

ABSTRAK

Dalam kajian ini, superkonduktor suhu tinggi $YBa_2Cu_3O_{7-\delta}$ (Y-123) telah disintesis melalui kaedah penguraian terma yang diubah suai menggunakan pelopor logam asetat dengan suhu pensinteran diubah antara 920 °C hingga 980 °C. Pembentukan fasa, mikrostruktur dan sifat superkonduktor telah dikaji secara sistematik. Analisis termogravimetri (TGA/DTG) menunjukkan proses penguraian berperingkat dengan pembentukan oksida terakhir berlaku pada suhu melebihi 500 °C. Analisis pembelauan sinar-X (XRD) mengesahkan Y-123 sebagai fasa dominan, disertai dengan fasa bendasing seperti Y_2BaCuO_5 (Y-211) dan $BaCuO_2$. Mikroskopi imbasan elektron (SEM) menunjukkan pertumbuhan butiran yang ketara daripada 0.85 μm kepada 1.36 μm apabila suhu pensinteran meningkat daripada 920 °C kepada 980 °C yang seterusnya meningkatkan keterhubungan antara butiran dalam sampel. Pengukuran rintangan elektrik menunjukkan bahawa semua sampel menunjukkan suhu kritikal onset ($T_{c\text{-}onset}$) yang tekal pada 93.1 K, manakala suhu sifar rintangan ($T_{c\text{-}zero)}$ meningkat daripada 75.1 K kepada 88.1 K apabila suhu pensinteran meningkat daripada 920 °C kepada 960 °C. Peningkatan dalam prestasi superkonduktor ini disebabkan oleh pembentukan fasa yang lebih baik dan peningkatan keterhubungan antara butiran. Keputusan ini menunjukkan bahawa pengoptimuman suhu pensinteran merupakan faktor utama dalam memperbaiki mikrostruktur dan sifat superkonduktor bagi sampel Y-123.

Kata kunci: Penguraian terma; pensinteran; superkonduktor; $YBa_2Cu_3O_{7-\delta}$

INTRODUCTION

High-temperature superconductors (HTS) are materials that exhibit zero electrical resistance and expel magnetic fields (Meissner effect) at temperatures typically above 77 K, the boiling point of liquid nitrogen. Hence, the discovery of HTS has revolutionised the field of

superconductivity by enabling more practical and cost-effective applications compared to conventional low-temperature superconductors, which require helium-based cooling (Bednorz & Muller 1986). Due to these advantages, HTS are widely explored for various usages (Hull 2003) such as power transmission cables (Foltyn et al. 2007; Larbalestier et al. 2001; Thomas et al. 2016), superconducting quantum interference devices (SQUIDs) (Wikswo Jr. 1995), and fault current limiters (Janowski et al. 2004). Among the HTS, $YBa_2Cu_3O_{7-\delta}$ (Y-123) remains as one of the most extensively studied compounds due to its ability to sustain high critical current densities (J_c) exceeding 10^6 A/cm^2 at 77 K (Foltyn et al. 2007; Larbalestier et al. 2001).

Various synthesis techniques have been developed to produce Y-123 samples, including solid-state (Hapipi et al. 2019), co-precipitation (Hapipi et al. 2018; Schildermans et al. 1999), thermal treatment (Dihom et al. 2017; Dzul-Kifli et al. 2022), and infiltration growth (Kamarudin et al. 2021). These methods significantly influence the superconducting properties of Y-123, as the phase formation and purity of the samples are highly dependent on the synthesis route and thermal treatment conditions. For example, the conventional solid-state method, which involve mixing and calcining oxide powders, often results in incomplete reactions, chemical inhomogeneities, and secondary phase formation, all of which can compromise superconducting performance (Bolzan et al. 1996; Hapipi et al. 2019). In contrast, wet chemical methods offer better chemical uniformity and lower synthesis temperatures, thereby producing finer, more homogeneous particles. However, these methods are generally more complex and require multiple processing steps. Therefore, as an effective alternative, a modified thermal decomposition method utilising metal acetate precursor has emerged (Arebat et al. 2025a, 2025b). This method promotes molecular-level mixing, resulting in more homogeneous precursor powders and a simpler process compared to other wet-chemical approaches. Furthermore, it allows for lower calcination temperatures and shorter processing times than conventional solid-state methods.

Heat treatment, particularly sintering, is a critical parameter in determining phase purity, grain connectivity, and the suppression of secondary phases in Y-123 (Arebat et al. 2025a; Hapipi et al. 2017). Insufficient sintering temperatures can lead to incomplete phase formation, while excessively high temperatures may cause phase decomposition (Wang et al. 2024). For instance, Y-123 samples sintered at 980 °C via solid-state method showed higher phase purity and better superconducting properties compared to those sintered at 920 °C (Arebat et al. 2025c). Higher sintering temperatures also promote grain growth, resulting in an increase in the critical temperature (T_c) value. Furthermore, the narrower transition width (ΔT_c) observed at higher sintering temperatures indicates better sample homogeneity (Arebat et al. 2025c). Previous studies investigated the effects of calcination and sintering temperature on Y-123 samples synthesised via modified thermal decomposition method at 920 °C, 950 °C, and 980 °C for 24 h. It was reported that increasing temperature from 920 °C to 980 °C increased the $T_{c\text{-zero}}$ from 87.74 K to 90.27 K, respectively. These findings suggest that higher sintering temperatures promote the formation of Y-123 phase, which is favourable for enhancing superconductivity (Arebat et al. 2025a).

Based on these findings, the Y-123 superconductor was synthesised in this study using a modified thermal decomposition method to systematically investigate the effect of sintering temperature on phase formation and superconducting properties. In contrast to the study by Arebat et al. (2025a), which varied both calcination and sintering temperatures, the present work focused solely on the sintering temperature to better understand its role in influencing the microstructure and superconducting behaviour. The sintering temperature range of 920-980 °C was selected to allow direct comparison with the previous work (Arebat et al. 2025a) in a more comprehensive manner. Two additional intermediate temperatures, 940 °C and 960 °C, were included to provide a more detailed evaluation of the effect of sintering temperature on Y-123 bulks. Furthermore, this study suggests that the increased hole concentration may account for the rise of the $T_{c\text{-zero}}$ with sintering temperature.

MATERIALS AND METHODS

SAMPLES PREPARATION VIA MODIFIED THERMAL DECOMPOSITION METHOD

High purity metal acetates, yttrium acetate tetrahydrate ($Y(CH_3COO)_3.4H_2O$, 99.9%, Alfa Aesar), barium acetate ($Ba(CH_3COO)_2$, ≥ 99% Alfa Aesar), and copper (II) acetate monohydrate ($Cu(CH_3COO)_2.H_2O$, ≥ 99%, Sigma Aldrich) were weighed in a stoichiometric ratio of (1: 2: 3) for Y: Ba: Cu. The powders were mixed and hand-ground for 30 min using a mortar and pestle to ensure homogeneity. The resulting mixture underwent a pre-calcination at 600 °C for 30 min to remove volatile components. The pre-calcined powders were then finely ground for 1 h and subsequently calcined at 910 °C for 24 h. After calcination, the powders were ground for 1 h and pressed into circular pellets (~13 mm in diameter and 2 mm thick) using a hydraulic press under a load of 5 tons. The pellets were sintered at various temperatures (920 °C, 940 °C, 960 °C, and 980 °C, respectively) for 24 h and slowly cooled to 600 °C for 12 h (annealing process) before further cooling to room temperature. All heat treatments, including calcination, sintering, and annealing, were carried out in a tube furnace under static air, with no gas flow. A consistent heating rate of 2 °C/min and a cooling rate of 1 °C/min were applied throughout the thermal processes.

CHARACTERISATIONS

The synthesised samples were characterised using several analytical techniques. Thermogravimetric analysis (TGA) and derivative thermogravimetry (DTG) were conducted using a Mettler Toledo thermobalance (model TGA/SDTA851ᵉ) with a heating rate of 5 °C/min to 1000 °C under a nitrogen atmosphere. Phase identification was performed using X-ray diffraction (XRD) with a PW 3040/ 60 MPD X'pert Pro Panalytical Philips DY 1861 x-ray diffractometer, employing Cu-Kα radiation source (λ = 1.5406 Å). XRD data were collected over the 2θ range of 20° to 80°, with a scanning step size of 0.03°. Grain morphology and elemental composition were examined using a scanning electron microscope (SEM-LEO 1455 VPSEM) equipped with an energy dispersive X-ray spectrometer (EDX). Temperature-dependent electrical resistance was measured using the standard four-point probe method in a closed-cycle helium cryostat. A constant current, I = 20 mA, was applied through the outer two probes, and the voltage (V) was measured across the inner two probes. The measurements were carried out over the temperature range of 30 K to 300 K. Resistance (R) was calculated using Ohm's law, V = IR, where V = voltage and I = current.

RESULTS AND DISCUSSION

THERMOGRAVIMETRIC ANALYSIS (TGA) AND DERIVATIVE THERMOGRAVIMETRIC (DTG)

Figure 1 shows the thermogravimetric analysis (TGA) and derivative thermogravimetric (DTG) curves of the precursor mixture. The mixture contains yttrium acetate tetrahydrate ($Y(CH_3COO)_3.4H_2O$), barium acetate ($Ba(CH_3COO)$), and copper acetate monohydrate ($Cu(CH_3COO)_2.H_2O$), prepared in a molar ratio of 1:2:3 before the pre-calcination process. For comparison, Figures 2, 3, and 4 show TGA and DTG curves of the individual raw powders of $Y(CH_3COO)_3.4H_2O$, $Ba(CH_3COO)$, and $Cu(CH_3COO)_2.H_2O$, respectively. In all graphs, the TGA curves (black line) represent the overall weight loss of the samples as a function of temperature, while the DTG curves (blue line) indicate the rate of weight loss (mg/min). As shown in Figure 1, the precursor mixture exhibits three major stages of weight loss within the temperature range of 50 °C to 1000 °C, corresponding to the stepwise decomposition of metal acetate into their respective oxides.

The first decomposition stage (Region R1, Figure 1) occurs between 57.47 °C and 172.03 °C, with an onset degradation temperature of 88.99 °C. This initial weight loss is attributed to the evaporation of surface-adsorbed moisture and the dehydration of $Y(CH_3COO)_3.4H_2O$ [1] and $Cu(CH_3COO)_2.H_2O$, which commonly takes place between 100 °C and 200 °C. Figure 2 confirms the thermal decomposition of ($Y(CH_3COO)_3.4H_2O$) between 58.42 °C and 217.40 °C, while Figure 4 shows $Cu(CH_3COO)_2.H_2O$ decomposes to $Cu(CH_3COO)_2$ between 59.37 °C and 179.70 °C. The experimentally observed mass loss of 8.67%, obtained directly from TGA results (Figure 1), is in good agreement with the theoretical value of 8.71%, calculated from the stoichiometric decomposition reactions based on the molecular weights of the reactants and their expected products:

$$Y(CH_3COO)_3.4H_2O \rightarrow Y(CH_3COO)_3 + 4H_2O \qquad (1)$$

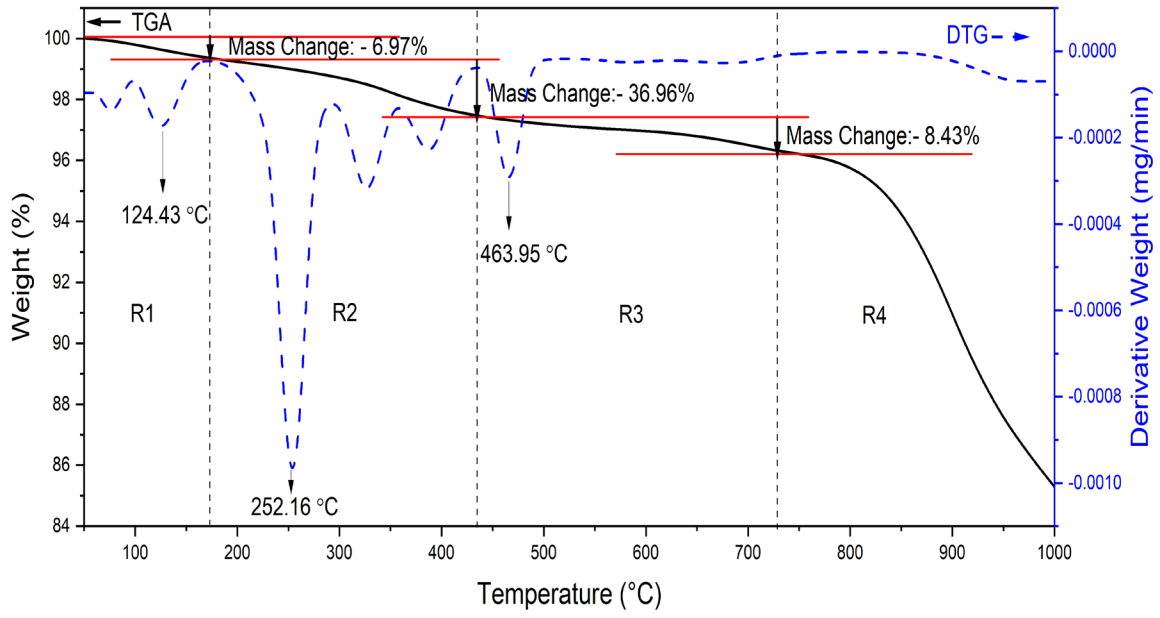

FIGURE 1. TGA/DTG profiles of uncalcined Y-Ba-Cu acetate precursor powder

$$3Cu(CH_3COO)_2.H_2O \rightarrow 3Cu(CH_3COO)_2 + 3H_2O \quad (2)$$

The second major degradation stage (Region R2, Figure 1) occurs between 173.58 °C and 436.92 °C, with a significant weight loss of 33.99% is observed. This value is close to the expected theoretical mass loss of 39.75%. This stage is associated with the decomposition of yttrium acetate ($Y(CH_3COO)_3$) and copper acetate ($Cu(CH_3COO)_2$), resulting in the release of acetic acid and carbon dioxide (CO_2). These reactions lead to the formation of yttrium oxide (Y_2O_3) and copper oxide (CuO):

$$Y(CH_3COO)_3 \rightarrow 1/2\ Y_2O_3 + 3/2\ (CH_3)_2CO + 3/2\ CO_2 \quad (3)$$

$$3Cu(CH_3COO)_2 \rightarrow 3CuO + 3(CH_3)_2CO + 3\ CO_2 \quad (4)$$

Figures 2 and 4 further confirm the complete decomposition of acetate groups and subsequent formation of Y_2O_3 and CuO, starting at 226.18 °C and 182.30 °C, respectively. Meanwhile, barium acetate ($Ba(CH_3COO)_2$) starts to decompose into barium carbonate ($BaCO_3$) at 241.41 °C:

$$2Ba(CH_3COO)_2 \rightarrow 2BaCO_3 + 2\ (CH_3)_2CO \quad (5)$$

The third decomposition stage (Region 3), observed between 437.44 °C and 513.22 °C, resulted in an additional weight loss of 5.97%, which closely matches the theoretical value of 6.08%. At this stage, $BaCO_3$ undergoes further decomposition to BaO, as supported by the data presented in Figure 2, where the second stage of weight loss is observed between 386.17 °C and 520.83 °C.

$$2BaCO_3 \rightarrow 2BaO + 2CO_2 \quad (6)$$

Beyond 513.22 °C, no further significant mass loss is observed, indicating complete decomposition and the formation of stable ceramic oxides. The final residue represents 51.37% of the initial mass, reasonably close to the theoretical value of 45.46% expected from the conversion of metal acetates into Y_2O_3, BaO, and CuO.

X-RAY DIFFRACTION (XRD) ANALYSIS

Figure 5 shows the XRD patterns of pure Y-123 samples prepared using modified thermal decomposition method. All samples exhibited prominent peaks corresponding to the $YBa_2Cu_3O_7$ phase (Y-123, ICSD: 98-005-0156) with an orthorhombic crystal structure and *Pmmm* space group. The most intense diffraction peaks were indexed to the (0 1 3) and (1 0 3) planes. Peaks corresponding to secondary phases such as Y_2BaCuO_5 (Y-211, ICSD: 98-002-4508) and barium cuprate ($BaCuO_2$, ICSD: 98-000-0514) were also observed in all samples. The presence of Y-211 is considered beneficial, as the Y-123/Y-211 interface can create defects that can act as flux pinning centres to improve the critical current density (J_c) of the samples (Jongprateep, Tangbuppa & Manasnilobon 2012; Kim & Hong 1999).

Table 1 shows the intensity fraction of each phase. The intensity fractions were estimated using the following formula:

$$YBa_2Cu_3O_{7-\delta}\ (\%) = \frac{\sum_{IYBa_2CusO_{7-\delta}}}{\sum_{IYBa_2CusO_{7-\delta}} + \sum_{IY_2BaCuO_5} + \sum_{IOther}} \times 100\% \quad (7)$$

where I is the peak intensity of the respective phases. At a sintering temperature of 920 °C, the intensity fraction of Y-123 phase is only 80.4%, while Y-211 and $BaCuO_2$ are 12.9% and 6.7%, respectively. This suggests that sintering at 920 °C was insufficient for complete phase formation. Limited atomic diffusion and the absence of oxygen flow at this temperature may cause incomplete reactions and promote secondary phase formation (Wang et al. 2024). As the sintering temperature increased to 940 °C and 960 °C, the Y-123 phase increased to 85.5% and 87.7%, respectively. Meanwhile, the amount of Y-211 and $BaCuO_2$ decreased, which indicates that higher temperatures promote more complete reactions and better phase purity. However, at 980 °C, the Y-123 content decreased to 79.5%, accompanied by an increase in secondary phases. The higher impurity levels at this elevated temperature suggests partial decomposition of Y-123 phase, likely due to oxygen loss from the Y-123 lattice. Without sufficient oxygen incorporation, the Y-123 structure became unstable and partially decomposed into Y-211 and $BaCuO_2$.

Table 1 summarises crystallite size calculated using Scherrer equation, based on the broadening of a relatively intense (103) peak of Y-123, using the following equation (Langford & Wilson 1978):

$$L = \frac{K\lambda}{B_{size} \cos\theta} \quad (8)$$

where L is the crystallite size; K is a dimensionless shape factor (0.9); B_{size} is the full width at half maximum (FWHM) in radian; λ is the X-ray wavelength for Cu-K_α radiation (1.5406 Å), and θ is the Bragg angle. Most samples exhibited a size of approximately 103.6 nm, indicating well-developed crystallites. However, the sample sintered at 920 °C had a smaller crystallite size of 73.7 nm, associated with broader peak (FWHM = 0.1624°). This broadening could be due to lattice distortion, microstrain, or incomplete crystallisation. As the temperature increased to 940 °C and above, the FWHM decreased to 0.1299°, and the crystallite size returned to 103.6 nm. This indicates the improvement of crystal growth and reduction of lattice strain at higher temperatures.

The lattice parameters (*a*-, *b*-, and *c*-axes) and unit cell volume were refined from the XRD data using HighScore Plus software. The *c*-axis values were subsequently used to estimate oxygen deficiency (δ),

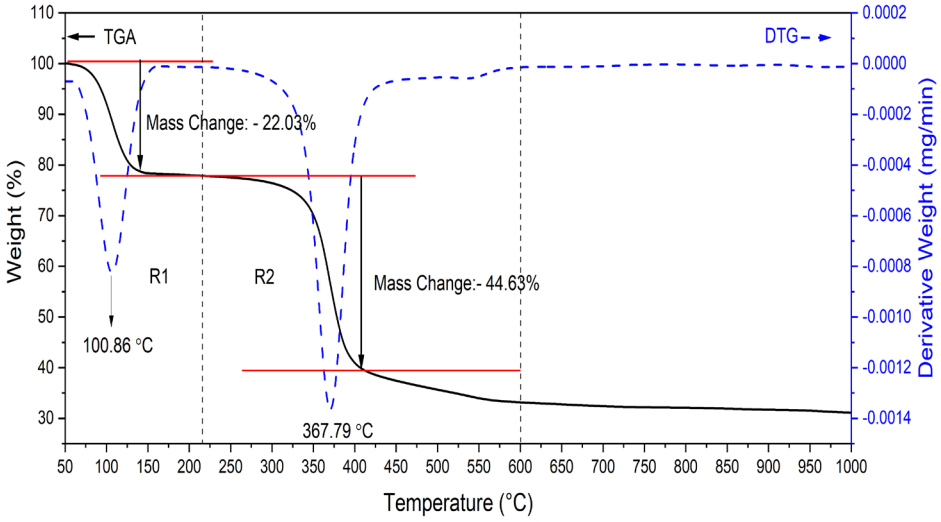

FIGURE 2. TGA/DTG profiles of raw yttrium acetate tetrahydrate ($Y(CH_3COO)_3.4H_2O$) powder

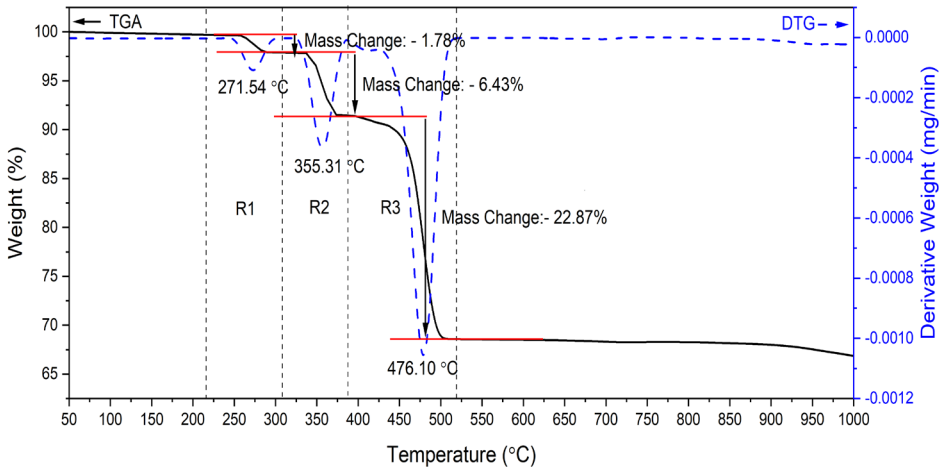

FIGURE 3. TGA/DTG profiles of raw barium acetate ($Ba(CH_3COO)$) powder

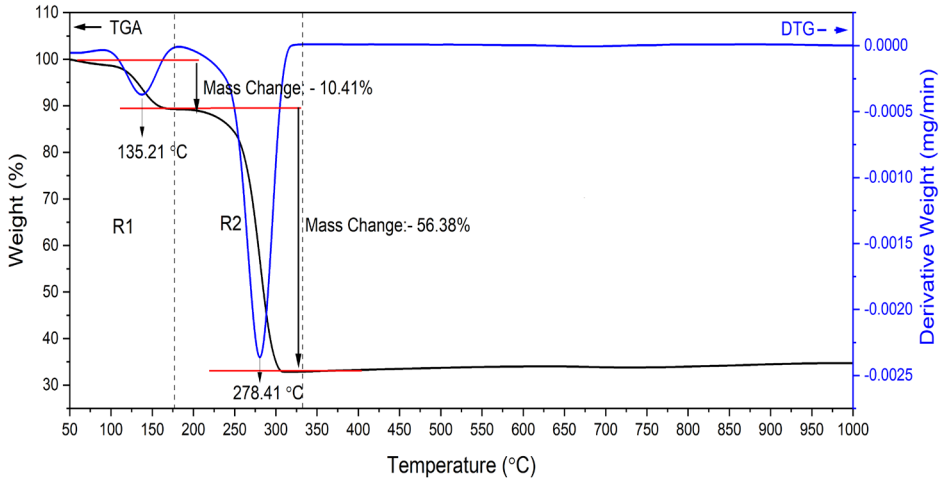

FIGURE 4. TGA/DTG profiles of raw copper acetate monohydrate ($Cu(CH_3COO)_2.H_2O$) powderSapictem re ipsus es aut ipsum ipsanduciis sequibus adicae net

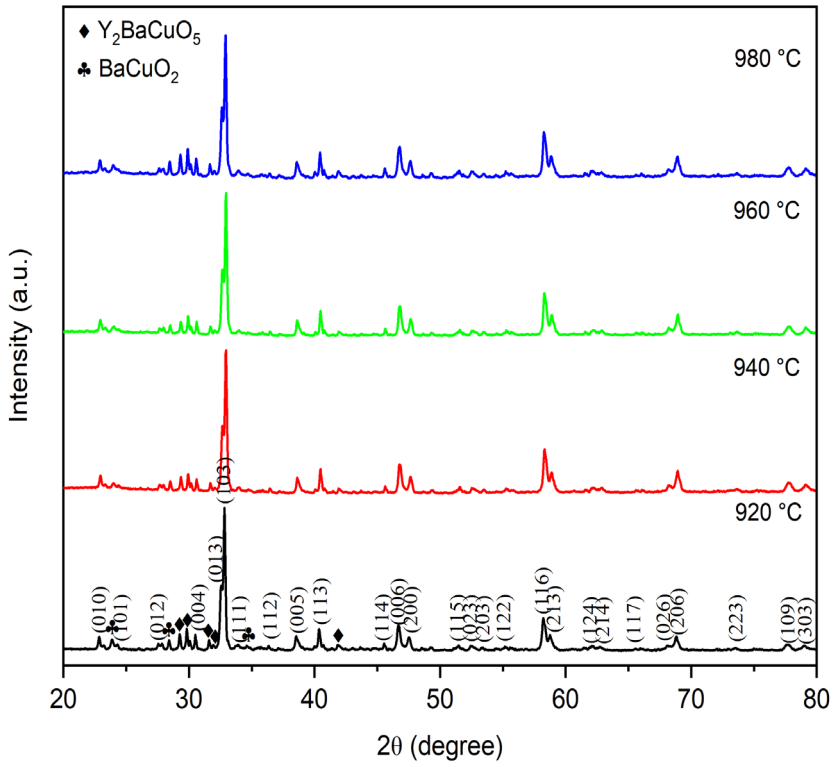

FIGURE 5. XRD patterns of Y-123 samples prepared using modified thermal decomposition method. The Y-211 and $BaCuO_2$ are marked with (♦) and (♣), respectively

as discussed in last section. All samples retained an orthorhombic crystal structure. The *a*-axis decreased slightly from 3.8262 Å to 3.8225 Å as the sintering temperature increased from 920 °C to 980 °C, possibly due to improved oxygen incorporation into the Cu-O chains (Benzi, Bottizzo & Rizzi 2004). In contrast, the *b*- and *c*-axes increased slightly, likely due to structural relaxation. The unit cell volume remained relatively constant, indicating that the overall crystal structure was stable throughout the sintering process.

MICROSTRUCTURE ANALYSIS

Figure 6 shows SEM images of fractured surfaces of Y-123 pellets sintered at various temperatures. The images show that the grains are randomly oriented with irregular shapes across all samples. At lower sintering temperatures of 920 °C and 940 °C, the grains appear smaller and separated by noticeable voids, indicating incomplete densification and weak grain connectivity. As the sintering temperature increases to 980 °C, the grains grow larger, and the grain boundaries become more compact, with significantly fewer voids. The average grain size of the samples was calculated using ImageJ software by analysing 100 randomly selected grains from each SEM image. The uncertainty values reported in Table 2 were calculated using the standard deviation formula. As shown in Table 2, the average grain size of the samples increased from 0.85 ± 0.03 µm at 920 °C to 1.36 ± 0.06 µm at 980 °C. This increase is attributed to a thermally activated diffusion mechanism, where higher temperatures provide sufficient energy for grain boundary migration and grain growth. Larger grain and enhanced grain connectivity are beneficial to superconducting properties, as excessive grain boundaries in Y-123 samples are known to impede the flow of supercurrent.

The elemental composition of the samples was examined using energy-dispersive X-ray spectroscopy (EDX). The EDX spectra shown in Figure 7 confirm the presence of yttrium (Y), barium (Ba), copper (Cu), and oxygen (O) in all samples, consistent with the expected $YBa_2Cu_3O_{7-\delta}$ stoichiometry. No foreign elements other than carbon (C) were detected, suggesting that the synthesis method successfully maintained the intended chemical composition across all sintering conditions. The appearance of carbon may be due to extrinsic factors, particularly the use of carbon tape during sample mounting.

T_C DEDUCED FROM TEMPERATURE DEPENDENCE OF ELECTRICAL RESISTANCE MEASUREMENT

Figure 8 shows the normalised resistance (R_T/ R_{300}) as a function of temperature for Y-123 samples sintered at different temperatures. All samples, except for the

TABLE 1. Intensity fraction of Y-123, Y-211, and $BaCuO_2$ phases, lattice parameters (*a*-, *b*-, and *c*- axes), unit cell volume, FWHM, and crystallite size of the samples sintered at various temperatures

Sintering Temp. (°C)	Intensity fraction (%)			Lattice parameters			Unit cell volume ($Å^3$)	FWHM (°) (103)	Crystallite size (nm)
	$YBa_2Cu_3O_{7-\delta}$	Y_2BaCuO_5	$BaCuO_2$	*a*-axis (Å)	*b*-axis (Å)	*c*-axis (Å)			
920	80.4	12.9	6.7	3.8262 ± 0.0003	3.8843 ± 0.0004	11.6791 ± 0.0012	173.58	0.1624	73.7
940	85.5	10.2	4.3	3.8251 ± 0.0003	3.8862 ± 0.0004	11.6813 ± 0.0014	173.64	0.1299	103.6
960	87.7	9.4	2.9	3.8239 ± 0.0003	3.8863 ± 0.0004	11.6834 ± 0.0013	173.63	0.1299	103.6
980	79.5	14.0	6.5	3.8225 ± 0.0003	3.8840 ± 0.0004	11.6795 ± 0.0015	173.40	0.1299	103.6

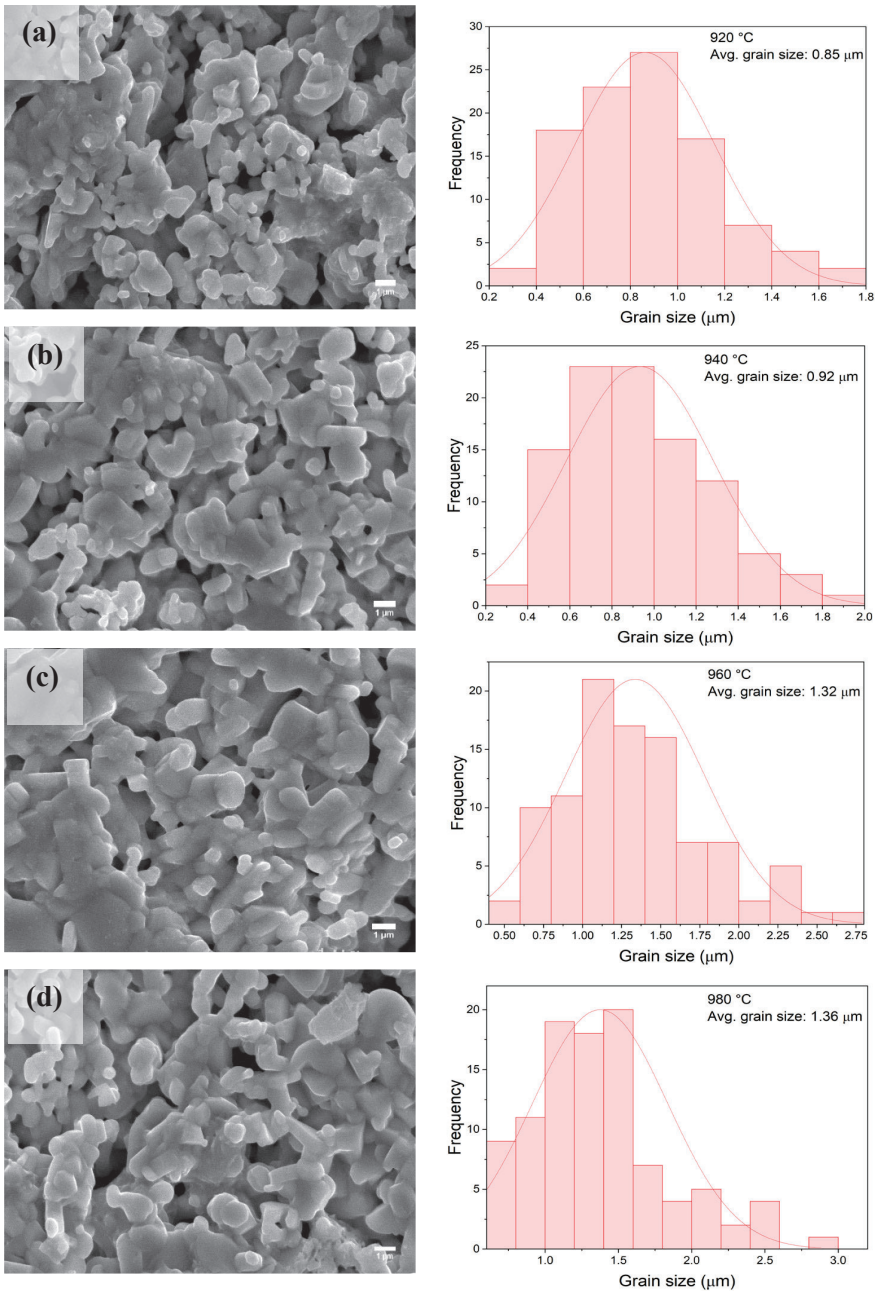

FIGURE 6. SEM images showing the fractured surfaces of Y-123 samples sintered at (a) 920 °C, (b) 940 °C, (c) 960 °C, and (d) 980 °C. Grain size distributions are displayed on the right-hand side of each image

TABLE 2. Average grain size of Y-123 samples sintered at different temperatures

Sintering Temp. (°C)	Average grain size (μm)
920	0.85 ± 0.03
940	0.92 ± 0.04
960	1.32 ± 0.05
980	1.36 ± 0.06

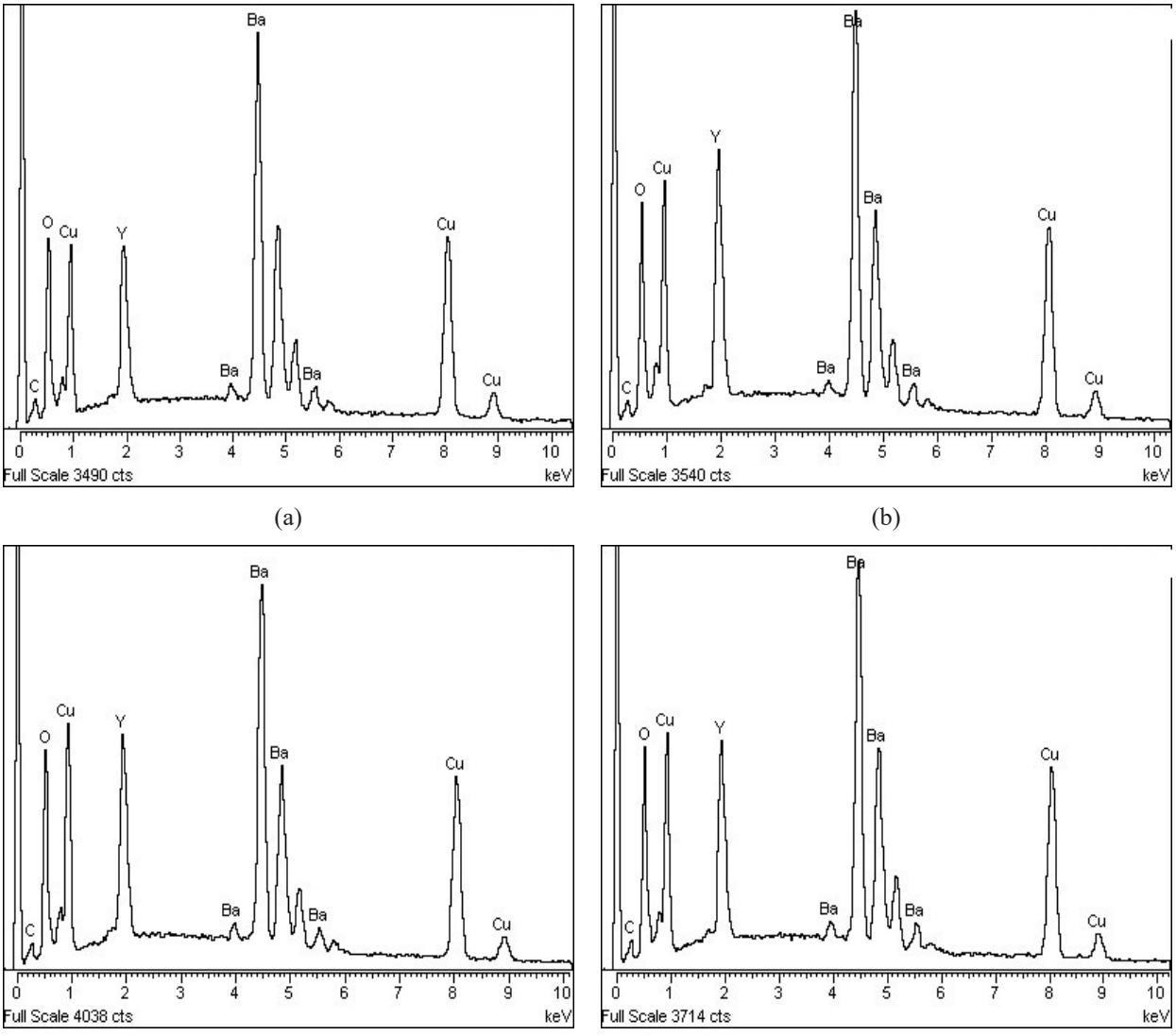

FIGURE 7. EDX spectra of fractured surfaces of Y-123 sample sintered at (a) 920 °C (b) 940 °C (c) 960 °C and (d) 980 °C

one sintered at 920 °C, exhibited metallic behaviour in the normal state above the onset of superconducting transition temperature ($T_{c\text{-onset}}$), followed by a sharp, single-step superconducting transition. This sharp transition indicates good grain connectivity and a homogeneous superconducting phase (Hamadneh et al. 2008; Hapipi et al. 2018). However, the sample sintered at 920 °C shows semiconducting behaviour above $T_{c\text{-onset}}$ and exhibited double-step transition to the superconducting state. This double-step transition is often attributed to the presence of secondary superconducting phases, weak intergrain coupling, or incomplete phase formation due to insufficient sintering temperature (Hapipi et al. 2022; Li et al. 2012; Nganga et al. 1990; Wang et al. 2024).

Figure 9 shows the derivative of resistance (δR/ δT) with respect to temperature, which was used to determine $T_{c\text{-onset}}$ and $T_{c\text{-zero}}$ (zero resistance) based on the inflection point of the plots. Table 3 shows that all samples have the same $T_{c\text{-onset}}$ value of 93.1 K, confirming the formation of Y-123 phase. However, $T_{c\text{-zero}}$ values varied significantly with sintering temperature. The sample sintered at 920 °C exhibited the lowest T_c-zero of 75.1 K and the broadest transition width (ΔT_c = 18.0 K), indicating the degradation of local homogeneity within the samples (Hapipi et al. 2018). As the sintering temperature increases to 940 °C and 960 °C, $T_{c\text{-zero}}$ improves to 86.1 K and 88.1 K, respectively, with narrower ΔT_c values, indicating better grain connectivity and improved superconducting phase homogeneity. Besides, the increase in grain size and reduction in voids as can be observed in Figure 6(c) also help to minimise grain boundary resistance and weak-link behavior that contribute to higher T_c values, However, at 980 °C, $T_{c\text{-zero}}$ slightly decreased to 85.1 K, possibly due to partial decomposition of the Y-123 phase and reformation of impurity phases, as indicated by the XRD results.

Table 3 also includes the estimated value of hole concentration (p), defined as the number of holes per Cu atom in the CuO_2 plane. It was calculated using the empirical relation (Presland et al. 1991; Tallon et al. 1995):

$$T_{c\text{-onset}} / T_{c\text{-max}} = 1 - 82.6\,(p - 0.16)^2 \qquad (9)$$

where p is the hole concentration; $T_{c\text{-max}}$ is the theoretical maximum transition temperature (93 K); and the value of 0.16 is the universal optimal hole concentration. As the sintering temperature increased from 920 °C to 940 °C, p increased from 0.137 to 0.144, suggesting improved oxygen incorporation into the Cu-O chains. This increase in oxygen content enhances hole doping in the CuO_2 planes, which increased the value of $T_{c\text{-zero}}$ from 75.1 K to 86.1 K, respectively (Matic & Lazarov 2007).

Additionally, the oxygen deficiency (δ) values were estimated using the empirical formula given by Benzi, Bottizzo and Rizzi (2004), based on the c-axis lattice parameter:

$$(7 - \delta) = 75.250 - 5.856c \qquad (10)$$

where $(7 - \delta)$ is the oxygen content and c is the c-axis lattice constant (in Å) obtained from XRD. This method provides a reliable, non-destructive estimation of oxygen content in the orthorhombic regime ($\delta \leq 0.5$). As the

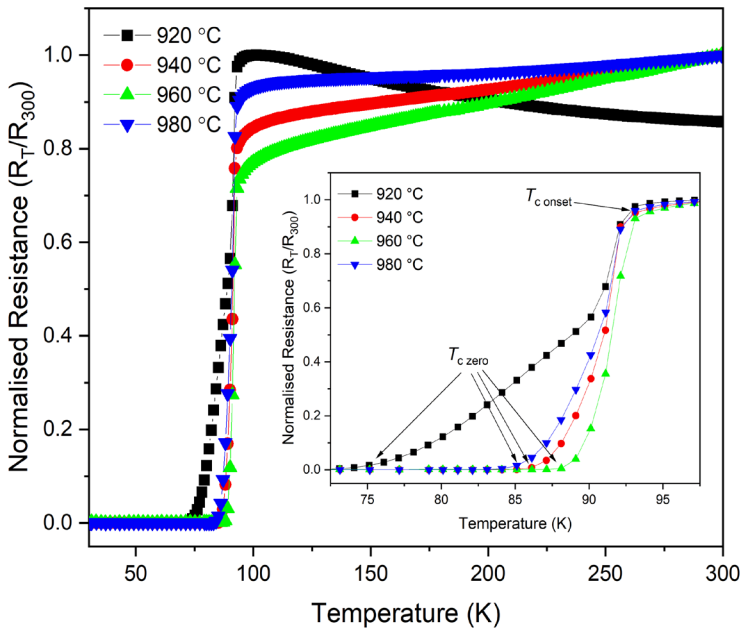

FIGURE 8. Normalised resistance versus temperature of Y-123 samples sintered at different temperatures. The inset highlights the enlarged region between 73 K to 98 K

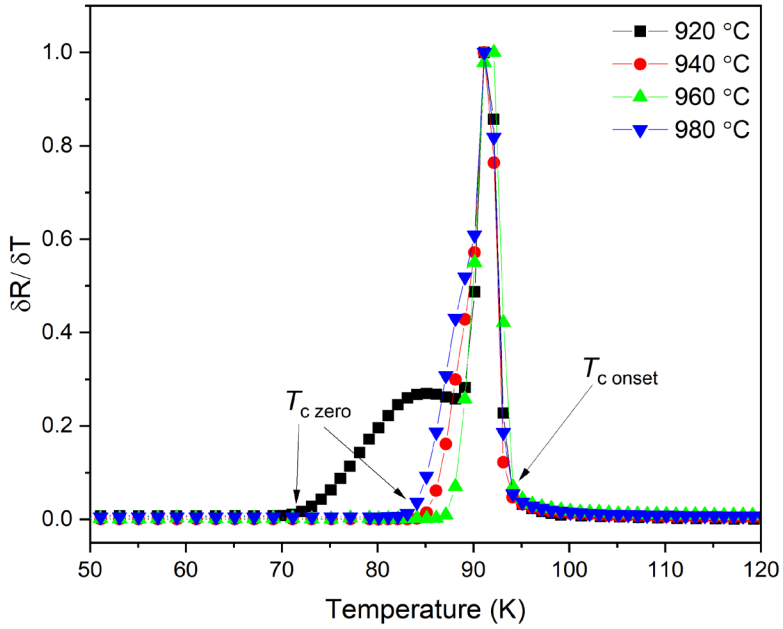

FIGURE 9. The derivative of resistance, δR/δT, against temperature of Y-123 samples sintered at different temperatures

TABLE 3. Superconducting transition parameters, hole concentration (p), c-axis lattice parameter, and estimated oxygen deficiency (δ) of Y-123 samples sintered at various temperatures

Sintering Temperature (°C)	$T_{c\text{-onset}}$ (K)	$T_{c\text{-zero}}$ (K)	ΔT_c (K)	Hole concentration, p	c-axis (Å)	Estimated oxygen deficiency, δ
920	93.1	75.1	18.0	0.137	11.6791	0.14
940	93.1	86.1	7.0	0.144	11.6813	0.16
960	93.1	88.1	5.0	0.144	11.6834	0.17
980	93.1	85.1	8.0	0.144	11.6795	0.15

sintering temperature increased from 920 °C to 960 °C, the estimated oxygen deficiency (δ) slightly increased from 0.14 to 0.17, suggesting gradual oxygen loss. Nevertheless, $T_{c\text{-zero}}$ still improved due to the dominant effect of enhanced phase formation and grain connectivity of the samples.

CONCLUSION

$YBa_2Cu_3O_{7-\delta}$ superconductors were successfully synthesised using a modified thermal decomposition method, with sintering temperatures varied at 920 °C, 940 °C, 960 °C, 980 °C. XRD analysis confirmed Y-123 as the major phase, with minor amounts of Y-211 and $BaCuO_2$. SEM analysis showed an increase average grain size from 0.85 ± 0.03 µm to 1.36 ± 0.06 µm for samples sintered at 920 °C and 980 °C, respectively, indicating enhanced grain growth at higher sintering temperature. The superconducting transition temperatures, especially $T_{c\text{-zero}}$, improved significantly with higher sintering temperatures, indicating enhanced phase homogeneity and grain connectivity of the samples. The optimal sintering temperature was found to be 960 °C, yielding the highest $T_{c\text{-zero}}$ of 88.1 K and the narrowest superconducting transition width (ΔT_c). These results highlight the effectiveness of sintering temperature optimisation in improving the structural and superconducting performance of Y-123 samples, supporting the viability of the modified decomposition method for high-quality superconductor fabrication.

ACKNOWLEDGMENTS

This research was funded by the Ministry of Higher Education Malaysia through the Fundamental Research Grant Scheme (FRGS/1/2023/STG05/UPM/02/6). The authors declare that they have no known competing financial interests or personal relationships that could have appeared to influence the work reported in this paper. Data will be made available upon request from the

corresponding author. Our contribution is as follows: Conceptualisation, N.M.H., S.K.C., and M.M.A.K.; Methodology, N.M.H., S.K.C., S.H.Y, X.T.H. and N.H.Y.M.A; Validation, N.M.H., S.K.C., O.J.L., A.H.S., M.M.A.K., K.P.L., M.K.S., K.B.T., and M.M.; Original draft preparation, N.M.H.; Writing-review and editing, S.K.C., K.B.T and O.J.L; Supervision, S.K.C.; Funding acquisition, S.K.C., O.J.L., A.H.S., M.M.A.K., K.P.L., and M.K.S.

REFERENCES

Arebat, R.A.M., Kechik, M.M.A., Baqiah, H., Chen, S.K., Lim, K.P., Shariff, K.K.M., Shaari, A.H., Yap, S.H., Sah, N.A.M.I.A. & Miryala, M. 2025a. Impact of calcination temperature on the microstructure and superconductivity of $YBa_2Cu_3O_{7-\delta}$ ceramic prepared via modified thermal decomposition method. *Journal of the Australian Ceramic Society* 61: 1375-1386.

Arebat, R.A.M., Kechik, M.M.A., Yap, S.H., Chen, S.K., Lim, K.P., Baqiah, H., Baarood, F., Humaidi, S., Peh, H.K., Shaari, A.H., Shabdin, M.K. & Miryala, M. 2025b. Sm_2O_3-induced superconductivity enhancements in bulk Y-123 ceramics synthesized via a novel modified thermal decomposition method. *Journal of Materials Research and Technology* 36: 9168-9181.

Arebat, R.A.M., Kechik, M.M.A., Chen, S.K., Lim, K.P., Peh, H.K. & Shaari, A.H. 2025c. Superconducting transition in YBCO bulk ceramics: Correlating sintering temperature, phase formation, and AC susceptibility. *Sains Malaysiana* 54(5): 1427-1437.

Bednorz, J.G. & Müller, K.A. 1986. Possible high T_c superconductivity in the Ba-La-Cu-O system. *Z. Physica B - Condensed Matter* 64: 189-193.

Benzi, P., Bottizzo, E. & Rizzi, N. 2004. Oxygen determination from cell dimensions in YBCO superconductors. *Journal of Crystal Growth* 269: 625-629.

Bolzan, A.A., Millar, G.J., Bhargava, A., Mackinnon, I.D.R. & Fredericks, P.M. 1996. A spectroscopic comparison of YBCO superconductors synthesised by solid-state and co-precipitation methods. *Materials Letters* 28: 27-32.

Dihom, M.M., Shaari, A.H., Baqiah, H., Al-Hada, N.M., Chen, S.K., Azis, R.S., Kechik, M.M.A. & Abd-Shukor, R. 2017. Effects of calcination temperature on microstructure and superconducting properties of Y123 ceramic prepared using thermal treatment method. *Solid State Phenomena* 268: 325-329.

Dzul-Kifli, N.A.C., Kechik, M.M.A., Baqiah, H., Shaari, A.H., Lim, K.P., Chen, S.K., Abd Sukor, S.I., Shabdin, M.K., Abdul Karim, M.K., Mohd Shariff, K.K. & Miryala, M. 2022. Superconducting properties of $YBa_2Cu_3O_{7-\delta}$ with a multiferroic addition synthesized by a capping agent-aided thermal treatment method. *Nanomaterials* 12(22): 3958.

Foltyn, S.R., Civale, L., Jia, Q.X., Maiorov, B., Wang, H. & Maley, M. 2007. Materials science challenges for high-temperature superconducting wire. *Nature Materials* 6: 631-642.

Hamadneh, I., Rosli, A.M., Abd-Shukor, R., Suib, N.R.M. & Yahya, S.Y. 2008. Superconductivity of $REBa_2Cu_3O_{7-\delta}$ (RE = Y, Dy, Er) ceramic synthesized via coprecipitation method. *Journal of Physics: Conference Series* 97: 012063.

Hapipi, N.M., Chen, S.K., Shaari, A.H., Kechik, M.M.A., Lim, K.P., Tan, K.B., Lee, O.J. & Miryala, M. 2022. Excess Mg *in situ* powder addition for enhancing critical current density of *ex situ* MgB_2. *Applied Physics A* 128(10): 913.

Hapipi, N.M., Lim, J.K., Chen, S.K., Lee, O.J., Shaari, A.H., Kechik, M.M.A., Lim, K.P., Tan, K.B., Murakami, M. & Miryala, M. 2019. Comparative study on AC susceptibility of $YBa_2Cu_3O_{7-\delta}$ added with $BaZrO_3$ nanoparticles prepared via solid-state and co-precipitation method. *Crystals* 9: 65.

Hapipi, N.M., Chen, S.K., Shaari, A.H., Kechik, M.M.A., Tan, K.B. & Lim, K.P. 2018. Superconductivity of Y_2O_3 and $BaZrO_3$ nanoparticles co-added $YBa_2Cu_3O_{7-\delta}$ bulks prepared using co-precipitation method. *Journal of Materials Science: Materials in Electronics* 29: 18684-18692.

Hapipi, N.M., Shaari, A.H., Kechik, M.M.A., Tan, K.B., Abd-Shukor, R., Suib, N.R.M. & Chen, S.K. 2017. Effect of heat treatment condition on the phase formation of $YBa_2Cu_3O_{7-\delta}$ superconductor. *Solid State Phenomena* 268: 305-310.

Hull, J.R. 2003. Applications of high-temperature superconductors in power technology. *Reports on Progress in Physics* 66: 1865-1886.

Janowski, T., Stryczewska, H.D., Kozak, S., Kondratowicz-Kucewicz, B., Wojtasiewicz, G., Kozak, J., Surdacki, P. & Malinowski, H. 2004. Bi-2223 and Bi-2212 tubes for small fault current limiters. *IEEE Transactions on Applied Superconductivity* 14: 851-854.

Jongprateep, O., Tangbuppa, P. & Manasnilobon, N. 2012. Compositions and particle sizes of $(RE)Ba_2Cu_3O_{7-x}$ superconductor powders synthesized by the solution combustion technique. *Advanced Materials Research* 488-489: 286-290.

Kamarudin, A.N., Kechik, M.M.A., Miryala, M., Pinmangkorn, S., Murakami, M., Chen, S.K., Baqiah, H., Ramli, A., Lim, K.P. & Shaari, A.H. 2021. Microstructural, phase formation, and superconducting properties of bulk $YBa_2Cu_3O_\gamma$ superconductors grown by infiltration growth process utilizing the $YBa_2Cu_3O_\gamma$ + $ErBa_2Cu_3O_\gamma$ + $Ba_3Cu_5O_8$ as a liquid source. *Coatings* 11(4): 377.

Kim, C.J. & Hong, G.W. 1999. Defect formation, distribution and size reduction of Y_2BaCuO_5 in melt-processed YBCO superconductors. *Superconductor Science and Technology* 12: R27-R41.

Langford, J.I. & Wilson, A.J.C. 1978. Scherrer after sixty years: A survey and some new results in the determination of crystallite size. *Journal of Applied Crystallography* 11: 102-113.

Larbalestier, D., Gurevich, A., Feldmann, D.M. & Polyanskii, A. 2001. High-T_c superconducting materials for electric power applications. *Nature* 414: 368-377.

Li, W.X., Zeng, R., Wang, J.L., Li, Y. & Dou, S.X. 2012. Dependence of magnetoelectric properties on sintering temperature for nano-SiC-doped MgB_2/Fe wires made by combined *in situ*/*ex situ* process. *Journal of Applied Physics* 111: 07E135.

Matic, V.M. & Lazarov, N.D. 2007. The origin of the 60 K plateau in $YBa_2Cu_3O_{6+x}$. *Journal of Physics: Condensed Matter* 19: 346230.

Nganga, L., Huong, P.V., Chaminade, J.P., Dordor, P., Frohlich, K. & Jergel, M. 1990. Influence of annealing under oxygen on the chemical and superconducting properties of $YBa_2Cu_3O_x$ single crystals. *Journal of the Less-Common Metals* 165: 208-214.

Presland, M.R., Tallon, J.L., Buckley, R.G., Liu, R.S. & Flower, N.E. 1991. General trends in oxygen stoichiometry effects on T_c in Bi and Tl superconductors. *Physica C* 176: 95-105.

Schildermans, I., Knaepen, E., Nouwen, R., Van Bael, M.K., Vanhoyland, G., Mullens, J., Yperman, J., Franco, D. & Van Poucke, L.C. 1999. Thermal treatment of a Y-123 precursor prepared using the hydroxide co-precipitation method. *International Journal of Inorganic Materials* 1(5-6): 351-355.

Tallon, J.L., Bernhard, C., Shaked, H., Hitterman, R.L. & Jorgensen, J.D. 1995. Generic superconducting phase behavior in high-T_c cuprates: T_c variation with hole concentration in $YBa_2Cu_3O_{7-\delta}$. *Physical Review B* 51: 911-914.

Thomas, H., Marian, A., Chervyakov, A., Stückrad, S., Salmieri, D. & Rubbia, C. 2016. Superconducting transmission lines – sustainable electric energy transfer with higher public acceptance? *Renewable and Sustainable Energy Reviews* 55: 59-72.

Wang, Y., Zhang, Z., Gao, Z., Wang, L. & Wang, Q. 2024. Exploring the preparation of $YbBa_2Cu_3O_{7-y}$ superconductor in flowing oxygen atmosphere. *Scientific Reports* 14: 8949.

Wikswo Jr., J.P. 1995. SQUID magnetometers for biomagnetism and nondestructive testing: important questions and initial answers. *IEEE Transactions on Applied Superconductivity* 5(2): 74-120.

*Corresponding author; email: chensk@upm.edu.my